Journal of Applied Polymer Science

Epoxy/Poly(ε-caprolactone) Nanocomposites: Effect of Transformations of Structure on Crystallization

Jaroslav Kratochvíl,[1] Jakub Rotrekl,[1,2] Ludmila Kaprálková,[1] Jiřina Hromádková,[1] Ivan Kelnar[1]

[1]Institute of Macromolecular Chemistry, Academy of Sciences of the Czech Republic, Heyrovského nám. 2, 162 06 Praha, Czech Republic

[2]Faculty of Chemical Technology, University of Pardubice, Studentská 95, 532 10 Pardubice 2, Czech Republic

Correspondence to: I. Kelnar (E-mail: kelnar@imc.cas.cz)

ABSTRACT: The influence of morphology of the epoxy/poly(ε-caprolactone) (PCL) system and corresponding nanocomposites with organophilized layered silicate on PCL crystallization was studied by differential scanning calorimetry, scanning, and transmission electron microscopy. The results obtained indicate a significant affecting of nonisothermal PCL crystallization by phase morphology brought about by the reaction-induced phase separation (RIPS) influenced either by various nanoclay contents or the epoxy/PCL ratio. Dispersed morphology of PCL matrix with epoxy globules induces crystallization at higher temperatures. The inverse dispersed morphology of epoxy matrix with PCL inclusions causes crystallization at lower temperature. The co-continuous morphology induces crystallization in both steps. Rate of the second crystallization step is substantially higher than that in the first step. No nucleation effect has been found in the nanocomposites with the added nanofiller. Multicomponent samples show retarded crystallization, i.e., lower crystallinities and lower overall crystallization rate compared with neat PCL. The results obtained suggest that it is primarily morphological/interfacial effects that play a decisive role in the crystallization behavior of PCL in the epoxy/PCL/clay system. © 2013 Wiley Periodicals, Inc. J. Appl. Polym. Sci. 130: 3197–3204, 2013

KEYWORDS: crystallization; morphology; composites; thermosets

Received 29 January 2013; accepted 11 May 2013; Published online 14 June 2013

DOI: 10.1002/app.39536

INTRODUCTION

Recently, an increasing number of papers indicates that existing methods to enhance toughness of epoxy thermosets consisting in the addition of elastomer-based and other polymeric modifiers can be successfully combined with the addition of various nanofillers.[1–10] The original motivation was elimination of most significant drawback of the mentioned toughening methods, i.e., reduced stiffness and strength.[11,12] In many cases, synergistic effect of the combination of both modifiers was found; this lead to simultaneous enhancement of all parameters or, at least, to higher toughness, which also resulted in possible reduced modifier content. This is of particular importance for high molecular-weight thermoplastic modifiers that cause increase in viscosity with corresponding limitation of the range of applications.[12] At the same time, thermoplastics may also be effectively applied to some progressive methods of *in situ* preparation of composites using soluble thermoplastic yarns stitched in, e.g., carbon fiber preform[13] or analogous thermoplastic films.[14]

An epoxy/thermoplastic system has significant dynamic asymmetry brought about by molecular weight/viscosity differences between its components. This leads to an asymmetric shape of phase diagram describing separation of originally dissolved polymer in the course of the reaction-induced phase separation (RIPS).[15–17] At the same time, this asymmetry can be effectively influenced by a selectively localized nanofiller.[7,18] We have found that an increasing nanofiller content can even lead to phase inversion of the epoxy/poly(ε-caprolactone) (PCL) system.[18] Thermoplastics used for epoxy toughening are mostly semicrystalline polymers such as poly(butyleneterephthalate), PCL, and poly(oxymethylene). Therefore, their mechanical performance is critically influenced by the crystalline phase type and content.[19] It is well understood that crystallization of modifying semicrystalline polymers is affected by both epoxy component[20] and nanofiller.[21–26] In spite of that, there are practically no studies revealing an effect of simultaneous presence of both the above mentioned components on crystallization behavior of the modifying polymer.

The existing studies of crystallization behavior of the epoxy/thermoplastic mixtures are predominantly focused on the systems with phase separated spherical inclusions of semicrystalline thermoplastics. The studies mostly include the effect of *in situ* formed epoxy network on crystalline phase formation, however, without evaluating the effect of the morphological type.[27–32]

Majority of works in this area are focused on blends of immiscible thermoplastics and other multiphase systems containing domains of polymer phase, where one or both components can crystallize. The effect of size of domains with globular or cylindrical shape on confined crystallization of polymers, including PCL and various copolymers, was also evaluated.[33–37]

The effect of morphological type on crystallization was demonstrated by comparison of the co-continuous and matrix/droplets structures formed either by reactive-compatibilization in polyethylene/polyamide blends[38] or by annealing the electrospun blend of polysulfone/poly(vinylidene fluoride).[39] With co-continuous structure, heterogeneous nucleation similar to the bulk sample occurred, whereas fractionated/homogeneous crystallization was found for isolated small droplets.

To the best of our knowledge, there is no study showing the influence of the structure formed by the clay-affected RIPS of the epoxy/thermoplastic modifier system on crystallization behavior. That is why this article deals with the effect of different clay contents and epoxy/PCL ratio on the structure and corresponding crystallization of PCL in the epoxy/PCL/nanoclay system.

EXPERIMENTAL

Materials

Cloisite C30 B (montmorillonite modified with methyl tallow bis(2-hydroxyethyl) quaternary ammonium chloride) was obtained from Southern Clay Products (Texas, USA). PCL m.w. 40,000 was obtained from Perstorp, Sweden. Diglycidyl ether of bisphenol A (DGEBA)-based epoxy resin Epilox A19-02 (Leuna-Harze GmbH, Germany), amine hardener 4,4′-diaminodiphenyl sulfone (DDS) (Aldrich, USA) were also used.

Preparation of Samples

The epoxy nanocomposites were prepared using a rotary mixer with an evacuated chamber. Epoxy, PCL, and the nanoclay (0–3 weight parts per hundred parts of resin (phr)), were mixed at 130°C for 60 min. Then, the curing agent was added (33 phr), and the mixing continued at the same temperature for 10 min. Test specimens (dog-bones and Charpy bars) were prepared by casting the sample into a steel mold and curing at 170°C for 4 h.

In the same way, a series of the PCL samples containing 1–5 wt % of liquid epoxy with stoichiometric amount of the hardener (and one sample without hardener) were prepared. These samples were divided into two parts—noncured and cured at 170°C for 4 h.

Differential Scanning Calorimetry

The differential scanning calorimetry (DSC) analysis was carried out using a Perkin-Elmer 8500 DSC apparatus. Cyclohexane, indium, and *n*-hexatriacontane were used to calibrate the instrument. The instrument was cooled with liquid nitrogen using an LN2 accessory at the set-point of −120°C and flushed with nitrogen as a purge gas. Samples of 5–10 mg were heated from 25°C to 230°C, cooled to −80°C, and reheated to 230°C at the heating/cooling rate of 10°C/min. The melting T_m and crystallization T_p temperatures were identified as the melting endotherm maximum and the crystallization exotherm minimum, respectively. The glass transition temperature T_g was identified as a mid-point between the glassy and rubbery branches of the DSC trace. Averages of the T_g values evaluated from the heating and cooling scans were used in the discussion below. The crystallinity was calculated using the value 139.3 J/g as heat of melting of 100%-crystalline PCL.[28] The nonisothermal crystallization (NIC) kinetics was evaluated from the crystallization exotherms of the DSC cooling runs using the Avrami approach.[40,41]

The Avrami equation reads:

$$X(t)=1-\exp\left(-kt^n\right) \quad (1)$$

where $X(t)$ is relative degree of crystallinity at time t, n is the Avrami exponent related to nucleation type and dimensionality of crystal growth, and k is the kinetic constant, which is a function of nucleation density and rate of crystal growth.

The results of 2–3 measurements were averaged in calculating the parameters of the DSC runs and the NIC kinetics.

Morphological Observations

The phase structure of the cryo-fractured samples was observed using scanning electron microscopy (SEM). The PCL phase was etched out with tetrahydrofuran for 1 h. The size of the dispersed particles was evaluated from the micrographs (from five representative pictures containing approximately 100 particles) using a Mini Mop image analyzer (Kontron, Germany).

For transmission electron microscopy (TEM), ultrathin (60 nm) sections were cut using an Ultracut UCT (Leica) ultramicrotome.

RESULTS AND DISCUSSION

Effect of Clay Content on Structure and Crystallization Mechanism

The samples of neat PCL, epoxy/PCL blends, and epoxy/PCL/C30 nanocomposites were scanned in the DSC heat–cool–heat cycle as described in the Experimental part. The results are summarized in Figures 1 and 3, and Tables I–III. Figure 1 shows DSC traces of NIC of the epoxy/PCL 80/20 (w/w) nanocomposites containing different amounts of the nanofiller scanned at the cooling rate of 10°C/min. The samples with increasing clay content correspond to the respective morphologies in Figure 2. The samples containing 1.5 phr (parts per hundred of resin) of clay fall, by chance, into a morphological transition region. As a result, the co-continuous structure [Figure 2(d)] and the inverse dispersed structure [Figure 2(e)] developed in the samples denoted 1.5a and 1.5b (Figure 1), respectively, because of possible minor fluctuations of composition and/or curing temperature during preparation.

The DSC cooling traces in Figure 1 indicate that, depending on the sample morphology changed with the clay content (see Figure 2), PCL in the epoxy/PCL 80/20 nanocomposites crystallizes on cooling by at least two different mechanisms characterized by two exotherms with minima at about +25°C and −40°C, respectively. The sample 0.0, i.e. the epoxy/PCL 80/20 blend containing no clay added, with the dispersed structure of large (∼20 μm) partially interconnected epoxy globules in the continuous PCL matrix [Figure 2(a)], shows a single narrow, symmetrical exotherm with the minimum at 26.3°C similar to that of neat PCL (Figure 3). This is probably a consequence of the fact that the sample (0.0 in Figure 1) has the morphology of the continuous PCL matrix

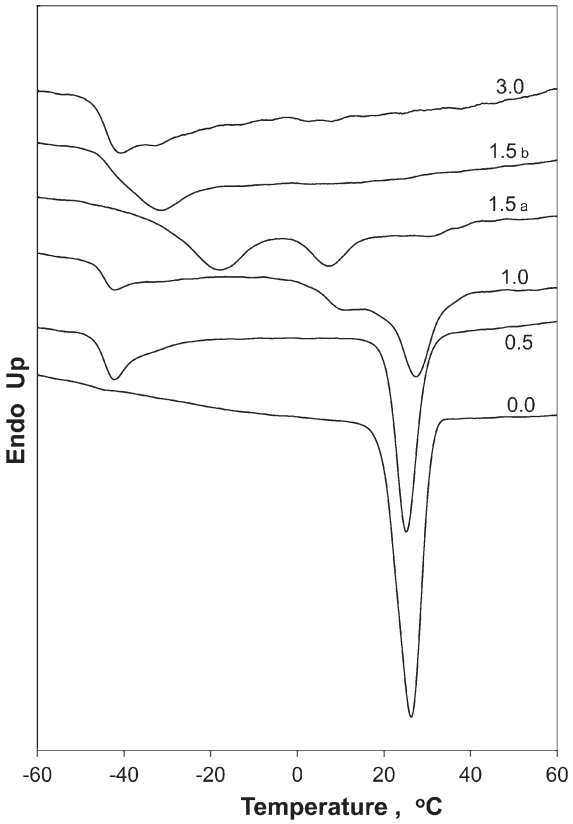

Figure 1. DSC thermograms of NIC of Epoxy/PCL nanocomposites 80/20 (w/w) containing C30 (phr values shown at respective traces).

where conditions are established for relatively free nonrestricted chain motion and formation of crystallization nuclei, similarly to bulk neat PCL. Therefore, PCL in sample 0.0 (Figure 1) obviously requires just a small undercooling to crystallize.

The other extreme is the sample containing 3 phr clay with the inverse dispersed structure of the fine PCL inclusions (~1 μm) in the epoxy matrix [Figure 2(f)]. The DSC trace (3.0 in Figure 1) shows an exotherm with the minimum at −41.5°C. Because of the absence of clay in the PCL phase detected by TEM (not shown), the reason of this behavior could be seen in the confinement effect of small PCL inclusions where the chains are restricted in their motion.[33−37] Consequently, crystallization requires higher driving force, i.e., greater undercooling, to run at its maximum rate. However, there is obviously another factor in play indicated by the fact that the exotherm of sample 3.0 (and also 1.5b—Figure 1) is not symmetrical but extended to higher temperatures. Obviously, during cooling, the crystallization in the sample with small PCL inclusions in the epoxy matrix starts as high as at about 0°C and then runs slowly to reach the maximum rate at about −42°C. It thus shows some kind of the fractionated crystallization.[38]

The samples denoted as 0.5, 1.0, and 1.5a have the rough co-continuous structure [Figure 2(b–d)]. This morphology includes both the above discussed structure types, i.e., threads of the continuous PCL matrix with the epoxy globules [Figure 2(a)] and the epoxy matrix with the fine PCL inclusions [Figure 2(f)]. Consequently, the samples with 0.5–1.0 phr clay show a combination of the two above discussed crystallization mechanisms demonstrated by two or more exotherms. The correspondence of crystallization mechanism and structure is well demonstrated by the DSC traces of the samples containing 1.5 phr C30. Sample 1.5a (Figure 1) has the co-continuous structure [Figure 2(d)] similar to that of samples with lower clay content [Figure 2(b,c)] and the DSC trace of this sample shows several exotherms. On the other hand, the sample of the same composition (1.5b) but different structure (see above) of the epoxy matrix with the PCL inclusions [Figure 2(e)], similar to that in Figure 2(f), shows the crystallization behavior similar to

Table I. NIC Characteristics of Nanocomposites PCL/Epoxy/C30

Sample			First heating		Cooling			Second heating		
Epoxy w_2	C30 phr	T_{g1} °C	T_m	CR %	T_{pa} °C	T_{pb} °C	CR %	T_m°C	CR %	T_{g2} °C
0.00	0.0	−63.1	63.6	52.8	31.4	-	49.3	57.8	45.5	-
0.80	0.0	−61.8	63.2	50.7	26.3	-	41.3	57.8	41.1	174.4
	0.5	−62.4	62.9	35.4	24.7	−42.4	35.2	59.8	37.7	173.4
	1.0	−63.4	62.8	34.5	26.9	−42.6	33.7	57.7	34.5	170.3
	1.5 a	−64.0	61.3	25.0	-	−18.1	35.8	57.4	33.7	169.4
	1.5 b	−63.8	59.2	17.1	-	−31.7	24.7	57.2	28.1	165.1
	3.0	−63.6	55.8	20.2	-	−41.5	23.5	56.4	27.2	156.4
0.85	0.0	−63.2	62.9	42.6	24.4	−24.0	39.0	58.1	40.7	182.4
	0.5	−63.9	60.7	43.1	-	−20.6	22.3	57.1	39.0	180.6
	1.5	−63.6	61.3	34.2	17.6	−13.8	30.7	57.3	34.6	175.9
	3.0	−63.3	57.8	26.5	-	−30.3	26.3	56.6	26.3	164.2
0.90	0.0	−62.5	57.1	45.9	-	−35.5	30.0	57.1	41.2	185.5

T_{g1}, T_{g2} glass transition temperature of PCL and epoxy.

T_m maximum of melting endotherm; T_{pa}, T_{pb} minimum of high- and low-temperature crystallization exotherms, respectively.

CR crystallinity normalized according to PCL weight fraction.

Table II. NIC Kinetics of Nanocomposites PCL/Epoxy/C30 Evaluated from High- (a) and Low-Temperature (b) Exotherms (see Figure 1)

Sample		Exotherm a			Exotherm b		
Epoxy w_2	C30 phr	n -	ln k s^{-n}	τ_{50} min	n -	ln k s^{-n}	τ_{50} min
0.00	0.0	2.72	−13.5	2.09	-	-	-
0.80	0.0	2.04	−12.4	6.06	-	-	-
	0.5	2.02	−12.7	7.47	2.28	−12.2	3.00
	1.0	2.04	−12.5	6.36	2.05	−11.8	4.42
	1.5 a	-	-	-	2.11	−12.1	4.34
	1.5 b	-	-	-	2.01	−11.5	4.27
	3.0	-	-	-	2.10	−11.5	3.34
0.85	0.0	1.88	−11.5	6.23	2.10	−10.5	2.10
	0.5	-	-	-	2.04	-12.0	4.96
	1.5	1.82	−11.2	6.37	2.24	−11.9	2.86
	3.0	-	-	-	2.10	−11.5	3.34
0.90	0.0	-	-	-	2.06	−12.0	4.96

n Avrami exponent; k crystallization rate constant; τ_{50} time of 50% relative crystallinity.

that of the sample with 3.0 phr clay. This confirms the idea of dominancy of morphological effects in the PCL crystallization mechanism.

Influence of Epoxy/PCL Ratio on Structure and Crystallization Mechanism

The series of samples of epoxy/PCL blends without clay has been studied with the purpose to support the above idea of dominant role of morphology in the crystallization behavior of PCL.

Figure 3 shows the DSC cooling traces of neat PCL and the epoxy/PCL blends. The crystallization of neat PCL is demonstrated by a narrow symmetrical exotherm with the minimum at 31.4°C. The sample containing 0.20 weight fraction of PCL (see also Figure 1—trace 0.0) has the dispersed structure of the epoxy inclusions in the PCL matrix [Figure 2(a)]. It shows a single crystallization exotherm similar to that of neat PCL, however, with the minimum at lower temperature 26.3°C. This seems to be a consequence of the two-phase system in which, because of the interfacial effects, motion of PCL chains is somewhat restricted and thus the crystallization requires higher driving force (undercooling). The sample with 0.10 weight fraction of PCL has the inverse dispersed morphology of the PCL inclusions in the epoxy matrix [Figure 4(a)] similar to that of the sample with 0.20 weight fraction of PCL containing 3 phr clay [Figure 2(f)]. As seen in Figures 1 and 3, the DSC cooling traces of both samples are quite similar. The crystallization exotherm of the sample 0.10 in Figure 3 is also broad with the minimum at greater undercooling −35.5°C and is also extended to higher temperatures.

The sample with the PCL weight fraction 0.15 in Figure 3 has the co-continuous morphology [Figure 4(b)] similar to that of the sample with 0.5 phr C30 [Figure 2(b)]. Their respective cooling traces in Figures 1 and 3 are quite similar. The sample 0.15 in Figure 3 also shows two separate exotherms with the minima at 24.4 and –24.0°C. These results indicate that the

Table III. Mixtures of PCL with Epoxy: DSC Runs and NIC Kinetics

			First heating		Cooling		Second heating		NIC		
Sample	Epoxy phr	T_{g1} °C	T_m °C	CR %	T_p °C	CR %	T_m °C	CR %	n -	ln k s^{-n}	τ_{50} min
PCL	0	−63.1	63.6	52.8	31.4	49.3	57.8	45.5	2.72	−13.5	2.09
Noncured	1	−62.8	60.5	48.7	25.7	46.0	56.3	45.8	1.71	−12.9	25.5
	3	−62.1	60.3	48.5	29.6	45.2	55.6	46.2	1.82	−13.2	19.1
	5	−61.1	62.0	47.6	30.1	44.6	55.1	45.6	1.96	−14.1	18.4
	5*	−61.9	61.4	49.4	28.3	45.5	55.9	44.5	1.83	−13.7	24.2
Cured	1	−61.8	58.0	46.8	26.6	42.8	55.7	44.5	1.82	−13.5	22.6
	3	−60.3	60.9	48.9	29.3	44.6	55.9	44.8	1.75	−13.3	26.9
	5	−59.1	60.2	48.6	30.0	43.2	55.5	45.2	1.85	−13.7	21.6

Symbols same as in Tables 1 and 2.
(5*) sample without hardener.

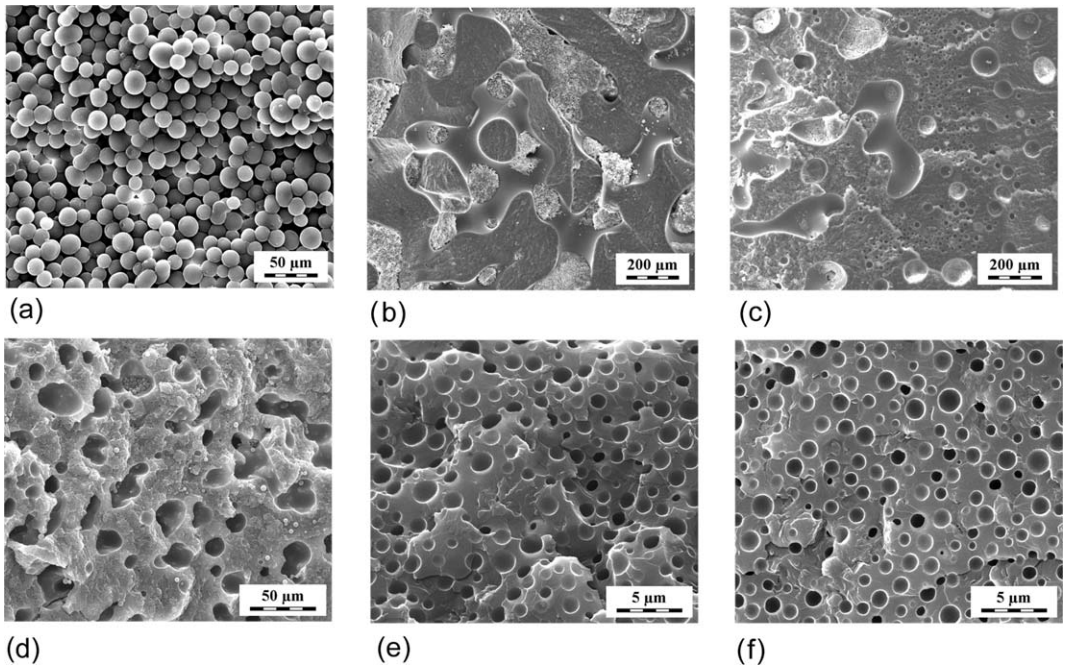

Figure 2. SEM images of structure of epoxy/PCL 80/20 in dependence on clay content (phr) (a) 0; (b) 0.5; (c) 1.0; (d,e) 1.5; (f) 3.0. Note that respective pictures have different magnifications—see the scale bars.

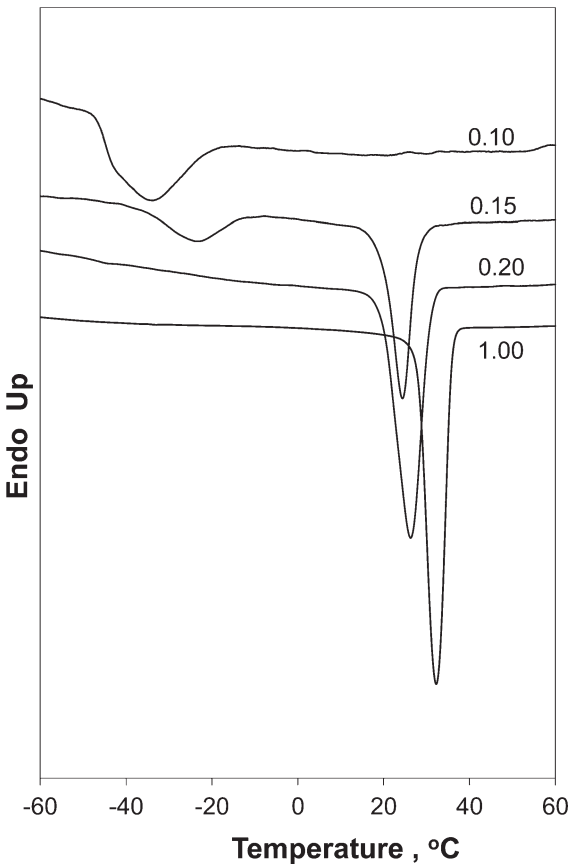

Figure 3. DSC thermograms of nonisothermal crystallization of PCL/Epoxy blends. Weight fractions of PCL are shown in the graph. The data were recalculated with respect to PCL weight fraction.

crystallization mechanism in the system epoxy/PCL/clay is primarily given by the structure/ morphology brought about by the composition- and/or clay-affected RIPS. It should be noted that our TEM study did not indicate the presence of clay in the PCL phase (not shown).

Evaluation of DSC Heating and Cooling Thermograms

Quantitative evaluation of the heating and cooling traces of the epoxy/PCL/clay nanocomposites is summarized in Table I. The samples show two glass transition temperatures—a characteristic feature of immiscible polymer blends. The low T_g of PCL falls within a narrow range between –62 and –64°C with no link-up to the sample composition. This indicates that the amorphous PCL domains, either in the matrix, droplets, or co-continuous structure, are, concerning the glass transition process, not influenced by the other two components (epoxy, clay) of the system and behave similarly to neat PCL.

On the other hand, the high T_g of cross-linked epoxy snows a marked dependence on the sample composition. In the samples with no clay, T_g decreases from 185.5°C to 182.4°C and to 174.4°C as the epoxy weight fraction decreases from 0.90 to 0.85 and 0.80, respectively. In the samples containing either 0.85 or 0.80 epoxy, T_g decreases steeply with the increasing content of clay. This is probably a consequence of the fact that the phase separation is hindered by the nanofiller[18] contained in the epoxy phase of the nanocomposites and that this phase also includes some portions of amorphous PCL. Both clay and PCL then reduce T_g of epoxy. These results comply with those obtained by the DMA method,[18] although the DSC values are generally somewhat lower.

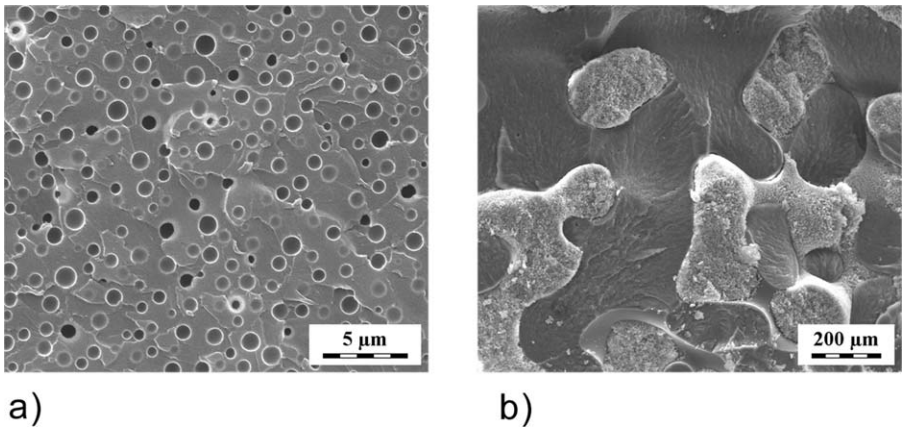

Figure 4. SEM images of epoxy/PCL containing (a) 10% PCL and (b) 15% PCL. For an image of 20% PCL sample see Figure 2(a). Note that respective pictures have different magnifications—see the scale bars.

All samples studied show single melting endotherms (not shown) in the first and second heating runs. As shown in Table I, T_m in the first run decreases both with decreasing content of PCL and with increasing weight fraction of clay. In the second run, this trend is less pronounced. The values of crystallinities show a similar trend. They also decrease from the highest value 52.8% of neat PCL with decreasing content of PCL in the system and also with the increasing weight fraction of clay. Crystallinities in the second heating run show somewhat lower values but, generally, the same trend. Moreover, there is a jump-like difference in the crystallinity values between the samples 1.5a and 1.5b having the same overall composition but different morphologies [Figure 2(d,e)]. The reason of this behavior could be seen in the morphological/ confinement effects discussed in the previous chapters.

The results of the DSC cooling runs do not suggest any nucleation effect of the added nanofiller that would be otherwise demonstrated by higher crystallization temperature T_p and higher crystallinity of the samples with clay.[42] On the contrary, the samples with added clay show lower T_p and lower overall crystallinities (sum of all exotherms) than neat PCL. Moreover, the samples with the inverse dispersion morphology of the PCL inclusions in the epoxy matrix, i.e., 80/20/1.5b, 80/20/3, and 90/10/0, show the low-temperature crystallization exotherm only.

These results, together with the above discussed results of T_g of PCL, suggest that it is morphological/interfacial effects that play a decisive role in the crystallization behavior of PCL in the epoxy/PCL/clay system. As mentioned above in discussing the T_g results, the amorphous PCL domains do not seem to contain significant portions of the other components of the system (epoxy, clay). The presence of clay in the epoxy phase only was confirmed also by TEM (not shown). Thus, the crystallization behavior should be primarily determined by morphological structure and surface phenomena taking place on the phase interface between the PCL and epoxy/C30 domains.

Kinetics of NIC

The NIC exotherms in Figures 1 and 3 have been treated by eq. (1). We are aware that not all assumptions of the Avrami theory[40] are met in such a complex heterogeneous system as epoxy/PCL/clay. Therefore, in the discussion below, we have to take eq. (1) just as a fitting tool allowing us to compare NIC kinetics in respective samples of the epoxy/PCL/clay system. Results of the Avrami treatment of the NIC kinetics are summarized in Figures 1 and 3. In line with requirements of the Avrami theory,[40] early stages, up to 30% relative crystallinity, at the most, have been taken into analysis.

The Avrami exponent n of the neat PCL shows the value 2.7 suggesting a three-dimensional growth, in compliance with other authors.[43,44] The n values evaluated from the high- and low-temperature exotherms (a and b in Table II) of the nanocomposites are around 2 indicating possible change in the growth mechanism from the three- to two-dimensional. This change could probably be induced by the two-phase character of the studied systems. The crystallization perhaps starts at the phase boundary and is thus affected by interfacial effects. However, this is not the only factor in play, as a possible small amount of dissolved liquid epoxy in the PCL phase has similar effect, as shown in the next section. Such changed crystal growth dimensionality from 3D spherulites to 2D axialites in similar systems has been described in the literature.[39,42,44]

The logarithm of the rate constant ln k (with time expressed in seconds, i.e. k in s^{-n}) shows the lowest value of -13.5 for neat PCL. The values for the nanocomposites evaluated from the exotherms in Figure 1 (Table II) are higher but do not show any dependence either on the epoxy/PCL ratio or on the content of clay. However, the rate constant k alone can only be used for comparing the crystallization rates if various samples show the same growth dimensionality, i.e., approximately the same n values, which is not our case.

A more appropriate variable is the time of reaching 50% relative crystallinity τ_{50}—a quantity inversely proportional to the overall rate of crystallization. Table II presents the values of τ_{50} calculated from n and k using eq. (1). The highest overall crystallization rate (lowest τ_{50}) has been found for neat PCL. In case of the epoxy/PCL samples, the crystallization rate evaluated from the high-temperature exotherm a is much lower (the τ_{50} values are on average about 3 times higher). This can be attributed to a hindered transport of polymer chains entangled on the

interface.[42] The overall crystallization rate evaluated from the low-temperature exotherm *b* is higher than that from exotherm *a*. Apparently, once the system overcomes a potential barrier where greater undercooling is necessary as a driving force,[38] the crystallization proceeds at a higher rate. Moreover, in the epoxy/PCL samples with the co-continuous morphology crystallizing in two steps, the overall rate of crystallization is much higher in the second step in the low-temperature region (exotherm *b*) than in the high-temperature region (exotherm *a*). Here, the crystallites formed during cooling in the first step function as nucleating centers and facilitate the second-step crystallization at a greater undercooling.

Effect of PCL Phase Composition

As we cannot exclude that the PCL phase in the prepared nanocomposite samples could contain some minor amount of dissolved noncrosslinked epoxy that would influence the crystallization behavior of PCL, we have prepared a series of the PCL samples containing defined concentrations of liquid epoxy (both with and without hardener) and tested them by the DSC method using the same protocol as for the above discussed nanocomposites.

Table III summarizes results of evaluation of the DSC heating and cooling thermograms, and the NIC kinetics of PCL with the addition of small amounts of epoxy and stoichiometric amount of the DDS hardener, and also one sample without hardener (5*). Moreover, the samples containing the hardener were also treated at 170°C for 4 h.

Unlike the above discussed systems containing high proportions of cross-linked epoxy, all the blends mentioned in Table III are miscible as documented by a single value of T_g. In the case of the noncured samples with hardener, the glass transition temperature increases with increasing amount of added liquid epoxy ($T_g \approx$ -40°C). The initial part of the T_g vs. composition curve can be fitted with the Gordon-Taylor equation with k = 1.65 documenting relatively strong specific interactions in the calculation. Here, OH groups of epoxy act as proton donors, and ester groups of PCL as proton acceptors in the hydrogen-bond interactions. Similar results have also been obtained for samples heated at 170°C. This suggests that this treatment probably resulted in linking between epoxy and DDS without formation of a cross-linked structure.

Compared with neat PCL, melting temperatures in the first and second heating runs of all epoxy-containing samples are lower, however, without any apparent dependence on either the sample composition or heat treatment. The values of crystallization temperature T_p and crystallinities are also lowered by the addition of epoxy. This suggests that the crystallization process is retarded even by small amounts of dissolved epoxy. Evaluation of the NIC kinetics (Table III) indicates possible change in the growth dimensionality from 3D in neat PCL to 2D in the blends. The overall crystallization rate in the blends as compared with neat PCL is dramatically reduced, as indicated by the values of τ_{50} calculated from n and k (Table III).

These results indicate that the decrease in crystallinities and reduction of crystallization rate in the epoxy/PCL/clay nanocomposites as compared with neat PCL could be caused, in addition to the droplet confinement/interfacial hindrance of chain mobility, also by the effect of interactions of PCL with possibly dissolved small amount of noncrosslinked epoxy. However, it is as yet impossible to estimate this effect as the amount of dissolved epoxy in the samples, if any, is not known.

CONCLUSIONS

The results indicate a significant affecting of nonisothermal PCL crystallization by phase morphology brought about by RIPS influenced either by various nanoclay contents or the epoxy/PCL ratio.

In the epoxy/PCL 80/20 system, the dispersed morphology of PCL matrix with epoxy globules induces NIC connected with the high-temperature exotherm (about +25°C). This process is slower than that in neat PCL. The inverse dispersed morphology of epoxy matrix with PCL inclusions brought about by 3 phr clay addition causes crystallization associated with the low-temperature exotherm (about −40°C). This process is somewhat faster than the previous one. The co-continuous morphology (clay content 0.5−1.0 phr) induces crystallization in two steps with both exotherms. Rate of the second crystallization step is substantially higher than that in the first step. Two samples of the same composition (1.5 phr clay) but different morphologies crystallize in the mechanisms characteristic for the respective structures.

The same three mentioned types of morphologies have also been detected in the epoxy/PCL mixtures with no clay added. The mixtures containing 20, 15, and 10 wt % PCL show the PCL matrix/epoxy globules, co-continuous, and epoxy matrix/PCL inclusions morphologies, respectively. These morphologies induce the same crystallization behavior as analogical structures in the epoxy/PCL (80/20)/clay system.

No nucleation effect has been found in the nanocomposites with the added nanofiller, which is in line with the finding that the nanofiller is contained in the epoxy phase only. In all multicomponent samples, PCL crystallization is retarded as shown by lower crystallinities and lower overall rates of crystallization as compared with neat PCL. The results obtained suggest that a decisive role in the crystallization behavior of PCL in the epoxy/PCL/clay nanocomposites is primarily played by morphological/interfacial effects. However, retardation of crystallization in the studied system could also be partially attributed to interactions of PCL with possible small amount of dissolved noncrosslinked epoxy.

ACKNOWLEDGMENTS

Contract grant sponsor: Grant agency of the Academy of Sciences of the Czech Republic (project No IAA200500904).

REFERENCES

1. Mirmohseni, A.; Zavareh, S. *J. Polym. Res.* **2010**, *17*, 191.
2. Bakar, M.; Kostrzewa, M.; Hausnerova, B.; Sar, K. *Adv. Polym. Technol.* **2010**, *29*, 237.
3. Kelnar, I.; Rotrekl, J.; Kaprálková, L.; Hromádková, J.; Strachota, A. *J. Appl. Polym. Sci.* **2012**, *125*, 3477.
4. Kelnar, I.; Rotrekl, J.; Kaprálková, L.; Hromádková, J. *J. Appl. Polym. Sci.* **2012**, *125*, 2755.

5. Zhang, J.; Xie, S. *Compos. B Eng.* **2011**, *42*, 2163.
6. Peng, M.; Li, D.; Chen, Y.; Zheng, Q. *J. Appl. Polym. Sci.* **2007**, *104*, 1205.
7. Peng, M.; Li, H.; Wai, L.; Chen, Y.; Zheng, Q.; Gu, W. *Polymer* **2005**, *46*, 7612.
8. Asif, A.; John, B.; Rao, V. L.; Ninan, K. N. *Polym. Int.* **2010**, *59*, 986.
9. Asif, A.; Leena, K.; Rao, V. L.; Ninan, K. N. *J. Appl. Polym. Sci.* **2007**, *106*, 2936.
10. Zhao, L.; Zhan, G.; Yu, Y.; Tang, X.; Li, S. *J. Appl. Polym. Sci.* **2008**, *108*, 953.
11. Frigione, M. E.; Mascia, L.; Acierno, D. *Eur. Polym. J.* **1995**, *31*, 1021.
12. Hodgkin, J. H.; Simon, G. P.; Varley, R. J. *Polym. Adv. Technol.* **1998**, *9*, 3.
13. Beier, U.; Wolff-Fabris, F.; Fischer, F.; Sandler, J. K. W.; Altstaedt, V.; Huelder, G.; Schmachtenberg, E.; Spanner, H.; Weimer, C.; Roser, T.; Buchs, W. *Compos. Pt. A Appl. Sci. Manuf.* **2008**, *39*, 1572.
14. Naffakh, M.; Dumon, M.; Gerard, J. F. *Compos. Sci. Technol.* **2006**, *66*, 1376.
15. Tanaka, H. J. *J. Phys. Condens. Matter.* **2000**, *12*, R207.
16. Yeganeh, J. K.; Goharpey, F.; Foudazi, R. *Macromolecules* **2010**, *43*, 8670.
17. Xia, T.; Huang, Y.; Peng, X.; Li, G. *Macromol. Chem. Phys.* **2010**, *211*, 2240.
18. Rotrekl, J.; Matějka, L.; Kaprálková, L.; Zhigunov, A.; Hromádková, J.; Kelnar, I. *Express. Polym. Lett.* **2012**, *6*, 975.
19. Galeski, A. *Prog. Polym. Sci.* **2003**, *28*, 1643.
20. Frensch, H.; Jungnickel, B. J. *Colloid Polym. Sci.* **1989**, *267*, 16.
21. Vo, L. T.; Giannelis, E. P. *Macromolecules* **2007**, *40*, 8271.
22. Wu, D.; Lin, D.; Zhang, J.; Zhou, W.; Zhang, M.; Zhang, Y.; Wang, D.; Lin, B. *Macromol. Chem. Phys.* **2011**, *212*, 613.
23. Miltner, H. E.; Watzeels, N.; Gotzen, N. A.; Goffin, A. l.; Duquesne, E.; Benali, S.; Ruelle, B.; Peeterbroeck, S.; Dubois, P.; Goderis, B.; Van Assche, G.; Rahier, H.; Van Mele, B. *Polymer* **2012**, *53*, 1494.
24. Ahmed, J.; Auras, R.; Kijchavengkul, T.; Varshney, S. K. *J. Food Eng.* **2012**, *111*, 580.
25. Ojijo, V.; Malwela, T.; Sinha Ray, S.; Sadiku, R. *Polymer* **2012**, *53*, 505.
26. Bandyopadhyay, J.; Sinha Ray, S.; Scriba, M.; Malwela, T. *Polymer* **2012**, *53*, 3602.
27. Zheng, S.; Zheng, H.; Guo, Q. *J. Polym. Sci. Pt. B Polym. Phys.* **2003**, *41*, 1085.
28. Guo, Q.; Groeninckx, G. *Polymer* **2001**, *42*, 8647.
29. Guo, Q.; Harrats, C.; Groeninckx, G.; Reynaers, H.; Koch, M. H. J. *Polymer* **2001**, *42*, 6031.
30. Oyanguren, P. A.; Frontini, P. M.; Williams, R. J. J.; Vigier, G.; Pascault, J. P. *Polymer* **1996**, *37*, 3087.
31. Goossens, S.; Groeninckx, G. *Macromolecules* **2006**, *39*, 8049.
32. Goossens, S.; Groeninckx, G. *J. Polym. Sci. Pt. B Polym. Phys.* **2007**, *45*, 2456.
33. Nojima, S.; Masashi, T.; Hara, S.; Tanimoto, S.; Sasaki, S. *Polymer* **2002**, *43*, 4087.
34. Akaba, M.; Nojima, S. *Polym. J.* **2005**, *37*, 584.
35. Nakagawa, S.; Kadena, K.; Ischizone, T.; Nojima, S.; Shimizu, T.; Yamaguchi, K.; Nakahama S. *Macromolecules* **2012**, *45*, 1892.
36. Jiang, S.; Ji, X.; An, L.; Jiang, B. *Polymer* **2001**, *42*, 3901.
37. Sanchez, M. S.; Mathot, V.; Poel, G. V.; Goeninckx, G.; Bruls, W. *J. Polym. Sci. Pt. B Polym. Phys.* **2006**, *44*, 815.
38. Córdova, M. E.; Lorenzo, A. T.; Müller, A. J.; Gani, L.; Tencé-Girault, S.; Leibler, L. *Macromol. Chem. Phys.* **2011**, *212*, 1335.
39. Zhong, G.; Su, R.; Zhang, L.; Wang, K.; Li, Z.; Fong, Z.; Zhu, L. *Polymer* **2012**, *53*, 4472.
40. Avrami, M. I. *J. Chem. Phys.* **1939**, *7*, 1103; II. Ibid **1940**, *8*, 212; III. Ibid **1941**, *9*, 177.
41. Supaphol, P. J. *J. Appl. Polym. Sci.* **2000**, *78*, 338.
42. Siqueira, G.; Fraschini, C.; Bras, J.; Dufresne, A.; Prud'home, R. *Eur. Polym. J.* **2011**, *47*, 2216.
43. L'Abee, R.; Van Duin, M.; Goossens, H. J. *Polym. Sci. Pt. B Polym. Phys.* **2010**, *48*, 1438.
44. Trujillo, M.; Arnal, M. L.; Müller, A. J.; Mujica, M. A.; De Navarro, C. U.; Ruelle, B.; Dubois, P. *Polymer* **2012**, *53*, 832.